Benchmarking the extraction of statistical neutron capture cross sections on short-lived nuclei for applications using the β-Oslo method

S. N. Liddick,[1,2,*] A. C. Larsen,[3] M. Guttormsen,[3] A. Spyrou,[1,4,5] B. P. Crider,[1] F. Naqvi,[1] J. E. Midtbø,[3] F. L. Bello Garrote,[3] D. L. Bleuel,[6] L. Crespo Campo,[3] A. Couture,[7] A. C. Dombos,[1,4,5] F. Giacoppo,[3,8,9] A. Görgen,[3] K. Hadynska-Klek,[3] T. W. Hagen,[3] V. W. Ingeberg,[3] B. V. Kheswa,[10,3] R. Lewis,[1] S. Mosby,[7] G. Perdikakis,[11,1,5] C. J. Prokop,[1,2] S. J. Quinn,[1,4,5] T. Renstrøm,[3] S. J. Rose,[3] E. Sahin,[3] S. Siem,[3] G. M. Tveten,[3] M. Wiedeking,[10] and F. Zeiser[3]

[1]*National Superconducting Cyclotron Laboratory (NSCL), Michigan State University, East Lansing, Michigan 48824, USA*
[2]*Department of Chemistry, Michigan State University, East Lansing, Michigan 48824, USA*
[3]*Department of Physics, University of Oslo, N-0316 Oslo, Norway*
[4]*Department of Physics and Astronomy, Michigan State University, East Lansing, Michigan 48824, USA*
[5]*Joint Institute for Nuclear Astrophysics, Michigan State University, East Lansing, Michigan 48824, USA*
[6]*Lawrence Livermore National Laboratory, 7000 East Avenue, Livermore, California 94550-9234, USA*
[7]*Los Alamos National Laboratory, Los Alamos, New Mexico 87545, USA*
[8]*Helmholtz Institute Mainz, 55099 Mainz, Germany*
[9]*GSI Helmholtzzentrum für Schwerionenforschung GmbH, D-64291 Darmstadt, Germany*
[10]*iThemba LABS, P.O. Box 722, 7129 Somerset West, South Africa*
[11]*Central Michigan University, Mount Pleasant, Michigan 48859, USA*

(Received 18 November 2016; revised manuscript received 6 June 2019; published 26 August 2019)

Numerous scientific fields including astrophysics, nuclear power, and nuclear forensics require a knowledge of basic nuclear properties for large numbers of short-lived, radioactive isotopes far removed from stable nuclei. Neutron-capture cross sections are one such piece of nuclear data where direct measurements are not possible and theoretical predictions can vary by orders of magnitude. A recently developed indirect technique for inferring neutron capture rates, the β-Oslo method, has been introduced but not compared against a known, directly measured neutron capture cross section. To provide this benchmark, two indirect methods based on β decay and charged-particle reactions were used to extract the nuclear level density and γ-ray strength function of ^{51}Ti. The nuclear level density and γ-ray strength function from the two data sets were found to be equivalent and were used to extract the neutron capture cross section of ^{50}Ti which agrees with previous direct measurements at high neutron energies. The results demonstrate the validity of the β-Oslo method for extracting neutron capture cross sections of short-lived nuclei and provide a sufficiently small uncertainty to be used in various applications.

DOI: 10.1103/PhysRevC.100.024624

I. INTRODUCTION

Basic nuclear reaction data, such as neutron capture reaction cross sections on short-lived isotopes, are critically important to a breadth of scientific fields. Elements heavier than iron ($Z = 26$) are created in various astrophysical environments either during the normal life of a star or through cataclysmic events with extreme neutron densities. The vast majority of the isotopes of the heavy elements are created in processes (s and r process) where neutron-capture reactions compete against β decay, and therefore accurate knowledge of both decay and reaction properties is critical [1,2]. Neutron star mergers were just confirmed as an r-process site [3–8], implying that neutron-capture cross sections are crucial for the final abundance pattern as an (n, γ)-(γ, n) equilibrium cannot be maintained at all times [9,10]. Neutron capture cross sections are needed to predict astrophysical elemental production important for cosmic chronometers, such as the Re/Os clock [11,12]. Neutron capture cross sections are also desired on a number of isotopes to optimize Gen-IV nuclear power reactor designs [13,14] and determine ideal parameters for the burn-up of nuclear waste [14,15], lessening the amount of material destined for long-term storage. Finally, neutron capture cross sections are needed to evaluate novel routes for medical isotope production, quantify elemental abundances from neutron activation analysis of rare or fragile objects, and for nuclear forensics.

Direct measurements of neutron capture cross sections are limited to stable nuclei and those with long half-lives. If applications require knowledge of neutron capture cross sections on unstable nuclei with short half-lives, direct measurements are precluded since the construction of either a target of neutrons or of short-lived radioactive isotopes is not currently feasible. Therefore, such applications resort to large sets of theoretically calculated reaction rates which are poorly constrained by experimental measurements, leading to orders of magnitude variations in predicted neutron capture cross sections just a few neutrons away from stability [16,17].

*liddick@nscl.msu.edu

To obtain neutron-capture cross sections, indirect methods have been developed which include the γ-ray strength [18], surrogate reaction [19,20], Oslo [21,22], and most recently, β-Oslo [23] methods. Even with these techniques, only a handful of reaction cross sections on short-lived isotopes have been determined (see, e.g., [16,24]). Only the β-Oslo method can be applied to nuclei produced at rates down to a few particles per second allowing indirect measurements of neutron capture rates further from stability. For this reason, it is important to validate the technique against a known, directly measured neutron capture cross section.

The Oslo, and β-Oslo methods extract the nuclear level density (NLD) and γ-ray strength function (γSF) from experimental data and use them to constrain a calculation of the neutron capture cross section using a statistical reaction model. The difference between the β-Oslo and Oslo methods lies in the population mechanism of β decay and charged-particle reactions, respectively. Radiative neutron capture is controlled primarily by three separate quantities: the interaction between the neutron and the target nucleus undergoing neutron capture, the residual nucleus' available quantum levels, and the respective decay properties of the levels populated in the (n, γ) reaction. The interaction between the neutron and the target nucleus can be accounted for by an appropriate optical model potential and there are relatively small changes in predicted neutron capture rates between different choices of the neutron optical model for nuclei relatively close to stability [16,25]. The other two quantities, the NLD and the average, γ-decay probability, the γSF, shed light on the dynamic behavior of the nucleus in the intermediate excitation-energy region. How these two quantities change as a function of both neutron and proton number is an open question [26–29], leading to orders of magnitude uncertainty in the calculated neutron capture cross section.

All of the indirect techniques must eventually be validated against directly measured neutron capture cross sections before widespread use in a particular application. This validation has been accomplished for the γSF [30], Oslo [31–33] and surrogate methods [20]. The β-Oslo method has not yet been validated. The technique has been used to extract (n, γ) cross sections for ^{75}Ge [23] and ^{68,69}Ni [16,34] but in both cases there was no previously measured neutron capture cross section for comparison. It could be assumed that the validation of the β-Oslo method derives from the validation of the Oslo method itself. However, the spin distributions populated following β decay or a charged-particle reaction are often not the same and the validity of the β-Oslo method cannot be immediately assured.

Herein, we present the application of both the β-Oslo and traditional Oslo methods to the extraction of the NLD and the γSF of ^{51}Ti from the ^{51}Sc $\rightarrow$ ^{51}Ti β decay and ^{50}Ti$(d, p)^{51}$Ti reaction. The resulting NLD and γSF are used to constrain the ^{50}Ti$(n, \gamma)^{51}$Ti cross section and compare it to previously measured data. It is demonstrated herein that the β-Oslo technique (1) is a valid means of determining neutron capture cross sections for short-lived isotopes, (2) agrees with the Oslo technique despite the differences in population mechanism, and (3) provides significantly reduced uncertainties in the (n, γ) cross section as compared to predictions where no data constraints are available, as is the case for many short-lived isotopes.

II. EXPERIMENTAL DETAILS

The β-decay experiment was performed at the National Superconducting Cyclotron Laboratory (NSCL). A primary beam of ^{86}Kr at 140 MeV per nucleon was impinged on a ^{9}Be fragmentation target. The resulting products were sent through the A1900 fragment separator [35] to isolate ^{51}Sc which was delivered to the experimental station. The incoming radioactive ion beam was characterized using standard energy-loss and time-of-flight measurements. The energy loss was taken from a 1-mm-thick Si PIN detector. The time of flight was measured using the same Si detector and a scintillator placed at a focal point of the A1900. The secondary ^{51}Sc ions were delivered at a rate of approximately 700 pps and the beam was greater than 90% pure.

The ^{51}Sc ions were deposited into a 1-mm-thick double-sided silicon strip detector (DSSD) segmented into 16, 1.2-mm strips on the front and back. The DSSD was used to record the position and time of arrival of the ^{51}Sc ions and their subsequent β decays. The β-delayed photons were monitored with the Summing NaI(Tl) detector (SuN) [36]. SuN is a 16-inch cylindrical volume of NaI(Tl), segmented into eight optically isolated segments with an inner bore hole of 1.7 inches in diameter. The β-Oslo method has been described previously [16,23,34] and only the salient features will be repeated here. SuN is used as a total absorption spectrometer; the sum of all γ-ray energy deposited into the detection volume provided the excitation energy E_x of the daughter state populated in β decay. The segmentation of SuN also allowed for the observation of individual γ-ray transitions E_γ within the cascades.

The decay of ^{51}Sc ($Q_\beta = 6.503$ MeV) populated high-energy states in the daughter nucleus ^{51}Ti. States above the neutron separation energy in ^{51}Ti ($S_n = 6.372$ MeV) were not observed to be populated. The total γ-ray energy emitted in the decay of the excited ^{51}Ti to the ground state was measured in SuN and plotted against the energies detected in the individual segments. The resulting $E_x - E_\gamma$ matrix contained contributions from both the parent ^{51}Sc decay ($t_{1/2} = 12.4$ s [37]) and daughter ^{51}Ti decay ($t_{1/2} = 5.76$ min [38–40]). To isolate the ^{51}Sc $\rightarrow$ ^{51}Ti β decay, the secondary ion beam was pulsed. The beam was delivered to the experimental station for 8 min and then turned off for 8 min. The time window between 3 and 8 min while the beam was off was used to obtain the total absorption spectrum for the daughter ^{51}Ti $\rightarrow$ ^{51}V decay. The ^{51}Ti decay was subtracted from the total spectrum based on the intensity of the strong 320-keV γ-ray transition between the $5/2^-$ and $7/2^-$ states in ^{51}V leading to the raw excitation energy as a function of γ-ray energy spectrum presented in Fig. 1(a).

The charged-particle ^{50}Ti$(d, p)^{51}$Ti experiment was conducted at the Oslo Cyclotron Laboratory (OCL), using a 3.5-nA deuteron beam at 12.5 MeV. A 1.08-mg/cm^2 ^{50}Ti target, 88% enriched in ^{50}Ti, with ^{48}Ti as the main contaminant, was used. The Q value of the reaction is 4147.92 keV [41].

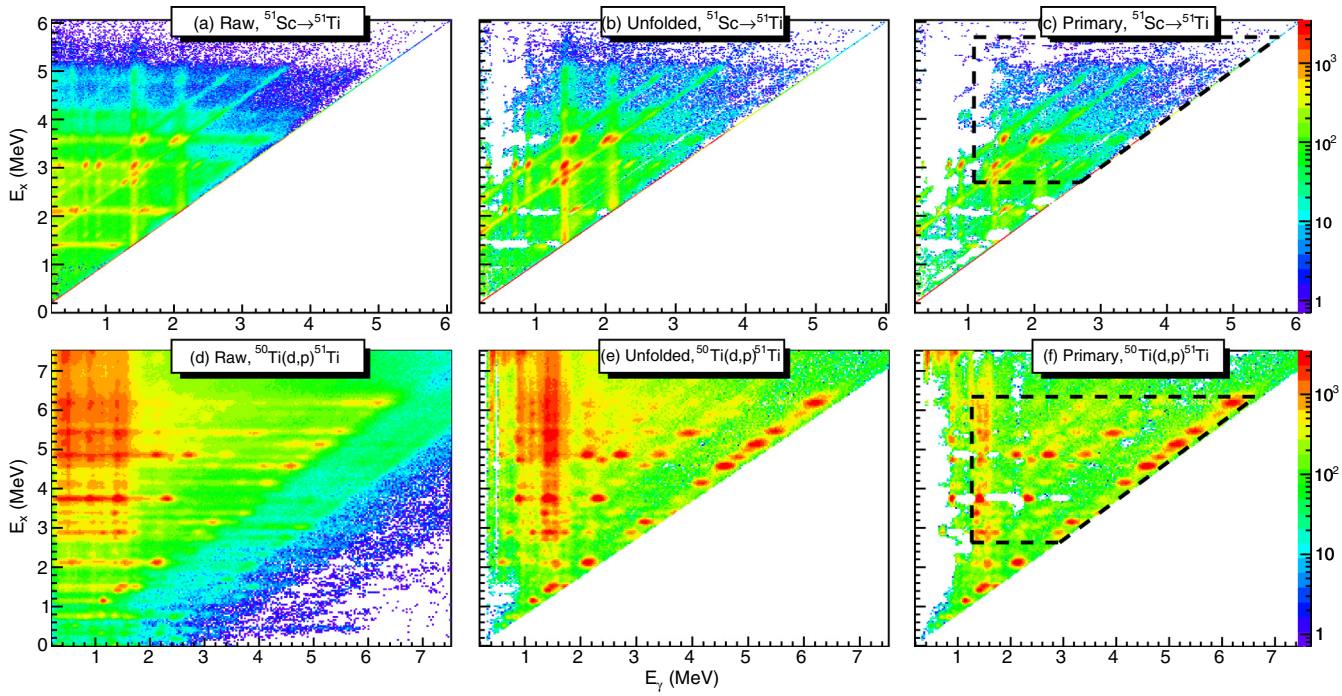

FIG. 1. (a) Raw experimental ^{51}Ti (E_γ, E_x) matrix from β decay of ^{51}Sc after subtraction of the daughter β decay of ^{51}Ti (see text for details). E_γ is the measured γ-ray energy in the NaI(Tl) segments of the SuN detector and E_x is the sum of all γ-ray energies (total absorption spectrum); (b) unfolded γ-ray distribution as a function of excitation energy from the β decay of ^{51}Sc; (c) primary γ-ray distribution from the β decay of ^{51}Sc. The area within the dashed, black line is used for the extraction of the NLD and γSF; (d) raw E_x vs E_γ matrix from the ^{50}Ti$(d, p)^{51}$Ti reaction; (e) unfolded γ-ray distribution as a function of excitation energy for the ^{50}Ti$(d, p)^{51}$Ti reaction; (f) primary γ-ray distribution from the ^{50}Ti$(d, p)^{51}$Ti reaction.

Charged particles were detected with the Silicon Ring (SiRi) [42], which comprises 64 individual $\Delta E - E$ telescopes, covering angles of 126–140° in the laboratory frame. Coincident γ rays were measured with the CACTUS NaI scintillator array [43]. The proton energy deposited in SiRi was converted to an excitation energy E_x in the residual ^{51}Ti nucleus using information on the reaction kinematics and the known Q value. The resulting $E_x - E_\gamma$ matrix is presented in Fig. 1(d). This matrix, together with the one in Fig. 1(a), are the starting points for the data analysis.

III. DATA ANALYSIS AND EXTRACTION OF LEVEL DENSITY AND γ-RAY STRENGTH

The known response functions of the SuN detector [36] and CACTUS [43] were used to unfold the excitation-energy tagged spectra using the technique described in Ref. [44]. The unfolded γ-ray matrices obtained in both the β decay and reaction data presented in Figs. 1(b) and 1(e) contain all γ rays from all possible decay cascades at a given excitation energy. The distribution of the first γ ray emitted in each cascade, i.e., the primary γ rays, can be obtained by an iterative subtraction technique detailed in Ref. [21]. The basic principle behind the technique is that a bin E_x will contain all γ rays from all cascades, while the lower energy bins $E_i < E_x$ will contain the same γ rays *except* the primary transitions from bin E_x to bin E_i. The underlying assumption is that the γ-ray deexcitation from a specific excitation energy bin is, on average, independent of whether the bin is reached through γ-ray population from higher excited states or through either the (d, p) reaction or β decay. The systematic errors associated with this procedure were detailed previously in Ref. [45].

The primary $E_x - E_\gamma$ matrices for the ^{51}Sc → ^{51}Ti β decay and the ^{50}Ti$(d, p)^{51}$Ti data are shown in Figs. 1(c) and 1(f). The areas within the dashed lines were used for the extraction of the NLD and γSF. The extracted NLD and γSF are not particularly sensitive to small changes in the specific location of the dashed line within approximately 500 keV on the excitation energy axis and 250 keV on the γ-ray energy axis as long as the lower limit on E_x is placed within a region of high level density and the lower limit on E_γ is placed above an energy where the extraction of the primary spectrum is known to have artifacts (see Ref. [45] for more details).

The intensity variation of the experimental, primary γ-ray spectra $P_{\rm exp}(E_x, E_\gamma)$ in Figs. 1(c) and 1(f) can be related to the NLD and γSF using [22]

$$P_{\rm exp}(E_x, E_\gamma) \propto \mathcal{T}(E_\gamma)\rho(E_x - E_\gamma), \tag{1}$$

where $\rho(E_x - E_\gamma)$ is the NLD at the excitation energy after the emission of the γ ray with energy E_γ, and $\mathcal{T}(E_\gamma)$ is the γ-ray transmission coefficient. The γ-ray transmission coefficient is related to the γSF, f, by

$$f(E_\gamma) = \frac{\mathcal{T}(E_\gamma)}{2\pi E_\gamma^3}, \tag{2}$$

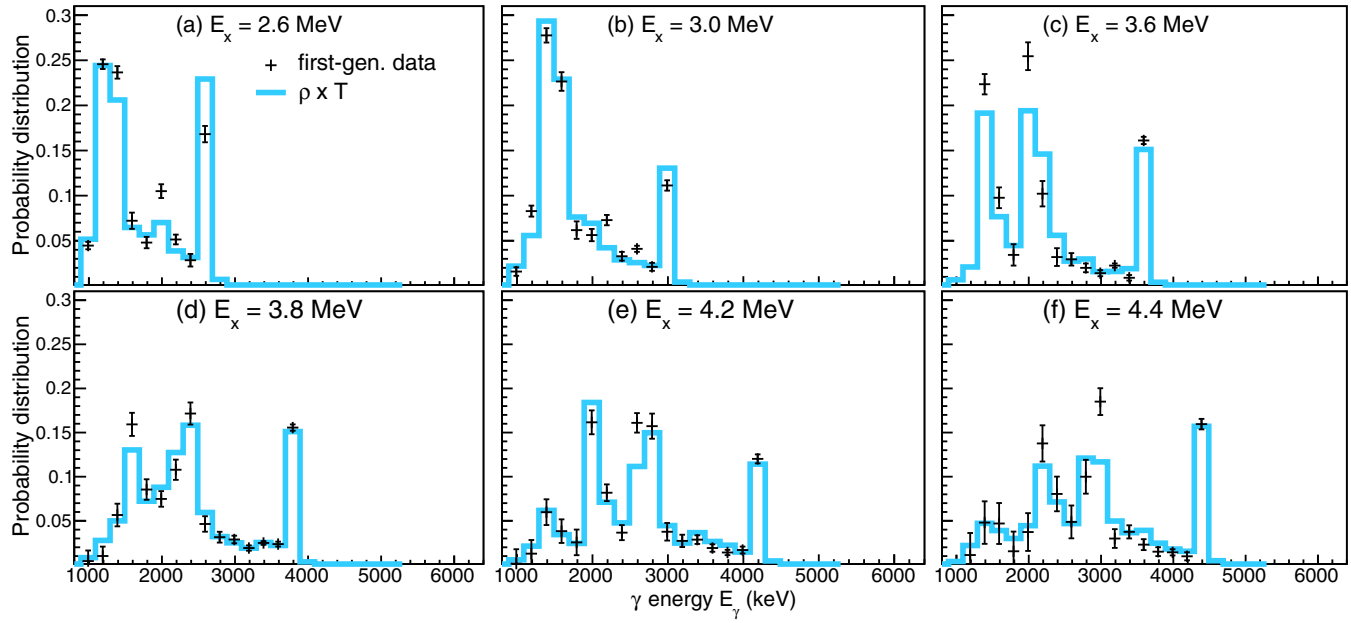

FIG. 2. Comparison of experimental, primary spectra extracted from the β-decay data (black crosses) to the calculated ones (light blue histogram) using the ρ and $\mathcal{T}$ functions obtained from the χ^2 fit. The comparison is performed for individual primary γ-ray spectra for a given $\approx$200-keV excitation-energy bin.

assuming that dipole radiation dominates, as supported by angular-distribution measurements in this mass region [46,47].

Using Eq. (1), one can approximate $P_{\rm exp}(E_x, E_\gamma)$ by $P_{\rm th}(E_x, E_\gamma)$, where

$$P_{\rm th}(E_x, E_\gamma) = \frac{\mathcal{T}(E_\gamma)\rho(E_x - E_\gamma)}{\sum_{E'_\gamma = E^{\rm min}_\gamma}^{E_x} \mathcal{T}(E'_\gamma)\rho(E_x - E'_\gamma)}, \tag{3}$$

where we have first normalized each experimental primary γ-ray spectrum to unity for each excitation-energy bin:

$$\sum_{E'_\gamma = E^{\rm min}_\gamma}^{E_x} P_{\rm exp}(E_x, E'_\gamma) = 1. \tag{4}$$

As shown in Ref. [22], if one solution $\rho(E_x - E_\gamma)$ and $\mathcal{T}(E_\gamma)$ of Eq. (1) is obtained, then one can construct an infinite set of equivalent solutions given by the transformation:

$$\widetilde{\rho}(E_x - E_\gamma) = A \exp[\alpha(E_x - E_\gamma)]\, \rho(E_x - E_\gamma), \tag{5}$$

$$\widetilde{\mathcal{T}}(E_\gamma) = B \exp[\alpha E_\gamma]\, \mathcal{T}(E_\gamma). \tag{6}$$

Any combination of values A, B, and α will yield solutions $\widetilde{\rho}$ and $\widetilde{\mathcal{T}}$ obeying

$$P_{\rm th}(E_x, E_\gamma) = \frac{\widetilde{\mathcal{T}}(E_\gamma)\widetilde{\rho}(E_x - E_\gamma)}{\sum_{E'_\gamma = E^{\rm min}_\gamma}^{E_x} \widetilde{\mathcal{T}}(E'_\gamma)\widetilde{\rho}(E_x - E'_\gamma)}. \tag{7}$$

However, it is important to stress that, for a given A, B, and α, the χ^2-minimization procedure gives a completely unique solution. Each (E_x, E_γ) bin used in the analysis gives one constraint to the fit. As an example, for the (d, p) data set, we have in total 304 (E_x, E_γ) bins within the dashed, black lines of Fig. 1(f) using a bin width of 195 keV. In contrast, we have 28 function values to be determined for $\rho(E_x - E_\gamma)$ and the same for $\mathcal{T}(E_\gamma)$, in total 56 free parameters. Hence, there are many more constraints than unknown and the fit is in fact overconstrained. Of course, this is only true if the Brink-Axel hypothesis [48,49] is fulfilled, so that the γ-ray transmission coefficient is a function of E_γ alone and not of E_x, as discussed in several other works [45,50,51].

In Figs. 2 and 3, examples of individual primary γ-ray spectra for a given excitation energy bin are shown. These spectra are compared to the calculated primary spectra using the ρ and $\mathcal{T}$ functions that are obtained from the χ^2 fit. Note that the individual spectra are taken at specific excitation-energy bins as marked in the panels, while the extracted functions are determined for the whole range of excitation energies within the dashed lines in Figs. 1(c) and 1(f). Overall, the product $\rho \times \mathcal{T}$ reproduces the experimental spectra very well, although some data points lie more than one standard deviation away from the calculated spectra. However, it should be noted that no attempts to include Porter-Thomas fluctuations [52] have been made, and as ^{51}Ti is a rather light nucleus with an overall low level density, such fluctuations are expected to be significant. Considering this fact, the agreement appears to be satisfactory.

To determine the slope α, and the scaling A and B, the usual approach has been to obtain these parameters using three experimental quantities: the known low-excitation-energy nuclear level density, the level density at the neutron separation energy $\rho(S_n)$, and the average, total radiative width $\langle\Gamma_\gamma\rangle$ [22,45].

In our case, the data were normalized based on quantities extracted from the existing level scheme of ^{51}Ti, the measured (γ, n) data on ^{50}Ti, and (n, γ) data on neighboring nuclei ^{46}Sc and ^{54}Cr. In the normalization procedure, no assumption was

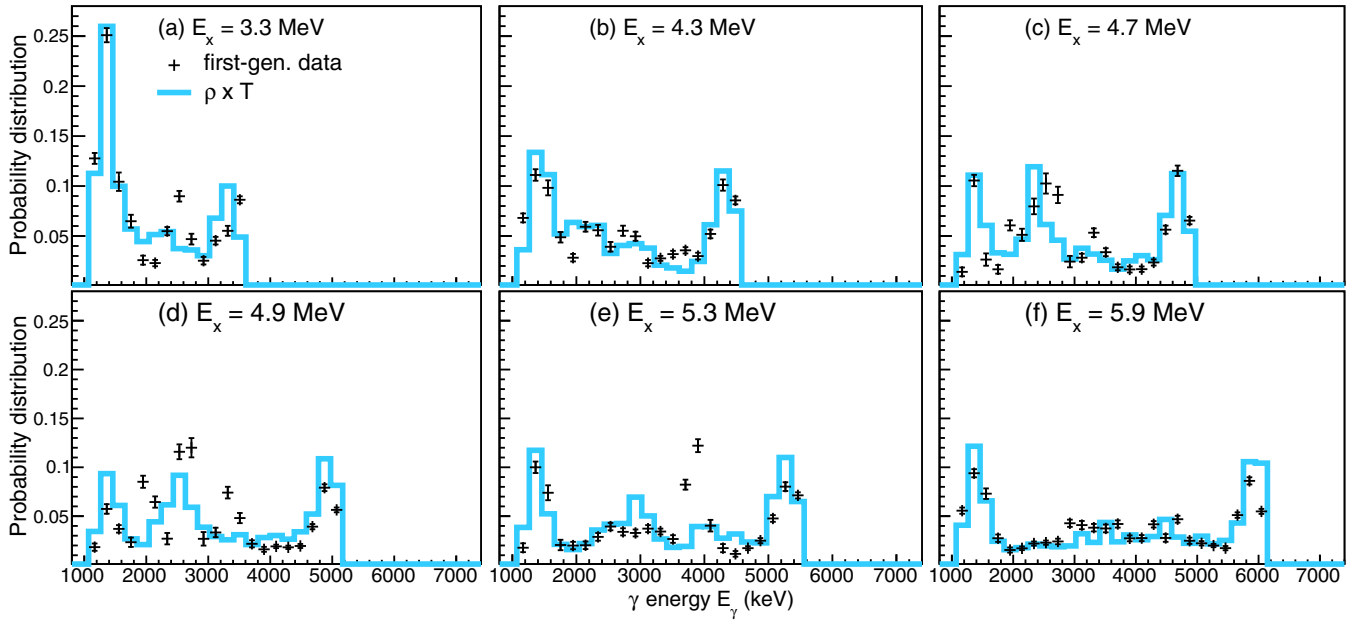

FIG. 3. Same as Fig. 2 but for the ^{50}Ti$(d, p)^{51}$Ti reaction.

made *a priori* on the value of $\langle\Gamma_\gamma\rangle$. $\rho(S_n)$ was deduced using the known level scheme of ^{51}Ti. This situation mimics the one encountered when extending the present method to more exotic isotopes for which little complementary experimental information exists. All known ^{51}Ti levels from the National Nuclear Data Center [53] database were used to create a cumulative distribution of levels as a function of excitation energy. This distribution was fit with a constant temperature model [54,55] from zero to a variable upper excitation energy limit in line with the approach in Refs. [28,29]. As demonstrated in Ref. [54], the constant temperature model is more appropriate for light nuclei than the Fermi-gas model. Also, in recent years, several authors have investigated the applicability of the constant-temperature model for nuclei in various mass regions; see, e.g., Refs. [56–62]. The best energy range was 0–3.5 MeV based on the quality of the fit to the cumulative level distribution as determined by the respective χ^2 values leading to a temperature T of 1.23(7) MeV and an energy shift E_0 of 0.0(2) MeV. Above ∼4 MeV, the level scheme of ^{51}Ti appears incomplete due to the deteriorating match between the constant temperature model and the cumulative level distribution taken from known data. A χ^2 fit to the noncumulative level density over a range from 0 to 3.5 MeV was also performed and resulted in values of $E_0 = 0.0(2)$ and $T = 1.3(1)$. Further, the suggested values of E_0 and T from RIPL3 [29] are 0.78(30) and 1.1(1), respectively. The values of $E_0 = 0$ and $T = 1.23$ were used for the remainder of the analysis.

The NLD for ^{51}Ti was normalized to the cumulative distribution of known levels up to 3.2 MeV for both the (d, p) and β-decay data, taking into account the fact that neither the (d, p) reaction nor β decay populates all known states. The ground state of ^{51}Sc is assigned spin/parity $(7/2^-)$ in the NNDC database [53]. However, from measured angular distributions of protons emitted from the ^{48}Ca$(\alpha, p)^{51}$Sc reaction [63], the $7/2^-$ assignment is indeed very convincing and we assume in the following that this is correct. Thus, through allowed (Gamow-Teller) β decay, the initial levels in ^{51}Ti have spin/parity $5/2^-, 7/2^-, 9/2^-$. Based on previous studies [53], levels with spin/parity $1/2^-$, $3/2^-$, $5/2^-$, $7/2^-$, $9/2^+$ are seen to be populated in the (d, p) and $(d, p\gamma)$ reactions, only considering levels with firm spin/parity assignments. Within the excitation-energy range 0–3.2 MeV, β decay and the (d, p) reaction each populate a subset of ≈73% of all observed levels. For the final levels reached by one γ-ray transition, assuming both $E1$ and $M1$ transitions, ≈78% of all observed levels are reached. Therefore, a reduction factor of ≈78% in the extracted level density is taken for both the β-decay data and the (d, p) reaction data. Since the reduction factor is based on a small number of levels there could be an additional uncertainty in the reduction factor as a function of excitation energy. It should be noted that this factor is extracted for the β-decay and (d, p) reaction independently and if only the β-decay data were known, the β-decay normalization would not be adversely impacted.

The upper normalization for the NLD was performed by fitting the experimental data points to the obtained CT level density in the E_x range 4.0–5.0 MeV and 3.7–3.9 MeV for the (d, p) data and β-decay data, respectively leading to a value for the level density at S_n of $\rho(S_n) = 146$ MeV^{-1}, corresponding to a $D_0 = 140$ keV. A spin cutoff parameter of $\sigma_J(S_n) = 3.12(11)$ taken from Eq. (16) in Ref. [64] was used in the level density calculation at S_n to correct for the subset of levels populated by β decay and the (d, p) reaction. It is assumed that σ_J^2 is a linear function of E_x as discussed in Ref. [65]:

$$\sigma_J^2(E_x) = \sigma_d^2 + \frac{E_x - E_d}{S_n - E_d}\left[\sigma_J^2(S_n) - \sigma_d^2\right]. \quad (8)$$

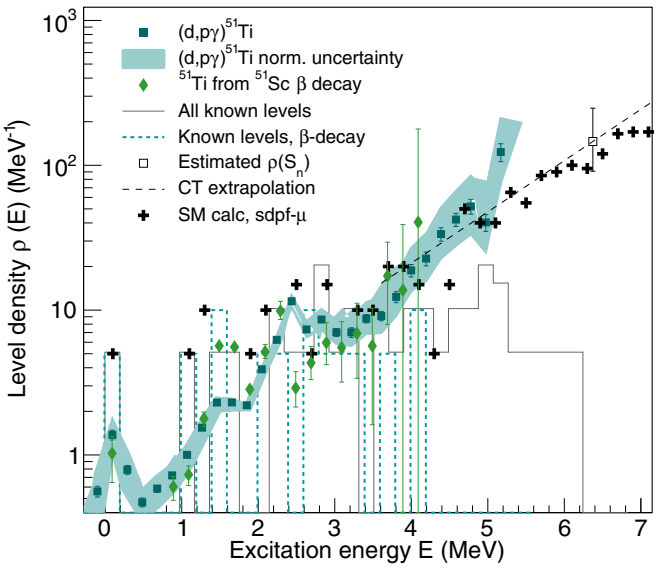

FIG. 4. Normalized nuclear level density of ^{51}Ti from the (d, p) reaction (dark cyan squares) and β-decay data (green diamonds). The bin widths are 200 keV/channel for the β-decay data and 195 keV/channel for the (d, p) data. The solid-line histogram shows known, discrete levels, while the dashed one shows the levels accessible for β decay after one dipole transition. The level densities are normalized to the cumulative distribution of levels taken from the known levels (see text for details). The cyan shaded band shows the uncertainty in absolute normalization for the (d, p) data; the error bars on the data points are due to statistical errors and uncertainties from the unfolding and primary γ-ray extraction. The absolute-normalization uncertainties are included in the error bars for the β-decay data. The systematic error bars for the β-decay and (d, p) data are similar. The shell-model level density is displayed as crosses.

The quantity $\sigma_d = 2.0$ is determined from known discrete levels [53] in the excitation energy region $E_d = 1.7 \pm 0.4$ MeV, where the level scheme is considered complete. Different models for the spin cutoff parameter $\sigma_J(S_n)$ leads to values ranging from 2.8 [55] to 3.4 [66]. The chosen value is in the middle of this range and the deviation has a small impact compared to other sources of error and is not considered further. Using the one-standard-deviation variations on T and E_0 in the constant temperature fit of the cumulative level distribution leads to a range of values for $\rho(S_n) = 91$–248 MeV^{-1} ($\pm 1\sigma$), corresponding to $D_0 = 225$–82 keV.

The resulting normalized level density is shown in Fig. 4. The error bars include statistical errors, systematic errors from the unfolding and the extraction of primary γ rays, and uncertainties in the normalization procedure. The shaded band shows the absolute-normalization uncertainty in the case of the (d, p) data, demonstrating that this is the largest contribution to the total uncertainty for the NLD at high excitation energies. It is interesting to note that various evaluations recommend very different values for the D_0 value of ^{51}Ti. Both the first and second version of the Reference Input Parameter Library, RIPL-1 and RIPL-2, give $D_0 = 125(70)$ keV [28,67], while the third version, RIPL-3, recommends $D_0 = 24.9(16)$ keV [29]. In the most recent *Atlas of Neutron Resonances* by Mughabghab [68], there is no D_0 value given, but from the list of resonances there are only four $\ell = 0$ resonances within an energy window of ≈330 keV, giving support to the rather large resonance spacing suggested in RIPL-1 and RIPL-2. We also note that the RIPL-1 and RIPL-2 value is quite close to our estimated value of $D_0 = 140$ keV from our best fit to the cumulative number of levels.

TABLE I. Experimental $E1$ and $M1$ strength functions from Ref. [28] used in the absolute normalization.

Nucleus	E_γ (MeV)	$E1$ 10^{-8}(MeV^{-3})	$M1$ 10^{-8}(MeV^{-3})	$E1+M1$ 10^{-8}(MeV^{-3})
^{46}Sc	7.1	1.6(6)	1.2(6)	2.8(17)
^{54}Cr	6.7	1.7(2)	0.59(6)	2.3(4)

The γSF was normalized to a simultaneous fit of the known ^{50}Ti(γ, n) data[1] [69] and the γSF extracted from the β-decay and (d, p) reaction data, in addition to the summed $E1$ and $M1$ strength functions obtained from (n, γ) reactions from RIPL-2 [28] for ^{46}Sc and ^{54}Cr (values are given in Table I). We used the following approach: (i) keeping the NLD normalization giving $\rho(S_n) = 146$ MeV^{-1}, a first, rough normalization was done by scaling the (d, p) γ-strength function so that the highest-E_γ data points roughly match the ^{46}Sc and ^{54}Cr data; (ii) the γ-strength function extracted from the β-decay data was scaled to the same absolute value as the (d, p) data in the range $E_\gamma \approx 4$–5 MeV; (iii) a phenomenological model (see below) was fit simultaneously to the β-decay and (d, p) data over the whole range of data points, as well as to the ^{50}Ti(γ, n) data and the ^{46}Sc and ^{54}Cr experimental strength functions. Steps (i)–(iii) were then repeated [improved scaling factor of the (d, p) data, improved scaling factor of the β-decay data, and performing a new fit] until a best fit was obtained as judged by the χ^2-square value. Then, to estimate strength-function uncertainties both due to the NLD normalization uncertainty and the uncertainty in the absolute scaling, we repeated the fits for each individual NLD normalization (low, middle, high) as well as for a low and high scaling of the γ-strength function. The starting point for the low scaling was the lower 1σ error of the ^{46}Sc RIPL-2 data point, while for the high scaling we used the upper 1σ error (see Table I).

To apply photoabsorption data for normalization of the γ-decay strength, we assume that the principle of detailed balance holds [70] so that $f^{\text{up}} = f^{\text{down}}$, as well as the Brink-Axel hypothesis [48,49], which implies that the strength function is independent of the spin/parity of the initial and final levels.

The fit function was composed of the sum of two generalized Lorentzian (GLo) functions for the $E1$ strength [71,72].

[1]Note that (γ, n) data are a good proxy for the γSF only when the neutron channel in the photoneutron data dominates.

The GLo model is given by

$$f_{\mathrm{GLo}}(E_\gamma, T_f) = \frac{1}{3\pi^2\hbar^2c^2}\sigma_{E1}\Gamma_{E1}\left[\frac{E_\gamma\Gamma(E_\gamma,T_f)}{\left(E_\gamma^2-E_{E1}^2\right)^2+E_\gamma^2\Gamma(E_\gamma,T_f)^2} + 0.7\frac{\Gamma(E_\gamma=0,T_f)}{E_{E1}^3}\right], \quad (9)$$

with

$$\Gamma(E_\gamma,T_f)=\frac{\Gamma_{E1}}{E_{E1}^2}\left(E_\gamma^2+4\pi^2T_f^2\right). \quad (10)$$

Here, the parameters Γ_{E1}, E_{E1}, and σ_{E1} correspond to the width, centroid energy, and peak cross section of the giant dipole resonance (GDR). The final states following γ-ray emission are assigned a constant nuclear temperature T_f so that the Brink-Axel hypothesis is regained [48,49].

In addition, two standard Lorentzian (SLo) components [48] were added to model the features at ∼14 MeV and account for the resonancelike structure observed in the (d, p) reaction data around S_n. The SLo model is

$$f_{\mathrm{SLo}}(E_\gamma)=\frac{1}{3\pi^2\hbar^2c^2}\frac{\sigma_{\mathrm{SLo}}\Gamma_{\mathrm{SLo}}^2E_\gamma}{\left(E_\gamma^2-E_{\mathrm{SLo}}^2\right)^2+\Gamma_{\mathrm{SLo}}^2E_\gamma^2}. \quad (11)$$

Here, the parameters Γ_{SLO}, E_{SLO}, and σ_{SLO} correspond to the width, centroid energy, and peak cross section of the respective features. The peak in the strength function observed at S_n is assumed to be dominantly $E1$ in character. Changing the assumption to $M1$ being dominant does not appreciably change the extracted cross section above $E_n \approx 200$ keV; however the average, total radiative width at S_n, $\langle\Gamma_\gamma\rangle$, is reduced significantly to about 500 meV compared to a value of 1240 meV obtained assuming $E1$. The peak structure is clearly visible in the matrices displayed in Figs. 1(d)–1(f) as a peak at $E_x \approx E_\gamma \approx 6$ MeV, i.e., on the diagonal representing direct decay to the $3/2^-$ ground state. We note that strong $M1$ spin-flip transitions have been observed via (p, p') reactions in very forward angles in this mass region [73,74]. For ^{50}Ti, there are $M1$ excitations with large cross section at $E_x \approx$ 5.7, 6.4, 7.3, and 8.0 MeV, and strong spin-flip $M1$ excitations at $E_x \approx 8.5$–11.0 MeV; see Figs. 1 and 2 in Ref. [73]. Therefore, it could well be that our phenomenological model fit in the region $E_\gamma \approx 7$–12 MeV underestimates the true strength for ^{51}Ti.

An upbend of the γSF is observed at low γ-ray energies similar to previous investigations in nearby Ti and Fe isotopes [75–77]. To describe the γSF below $E_\gamma = 4$ MeV an exponential form $f_{\mathrm{upbend}}^{M1} = C\exp(-\eta E_\gamma)$ is used and is assumed to be $M1$ in character based on shell model studies of the Ti isotopes [78] and the shell model calculations presented later. The total dipole-strength fit function is given by

$$f_{\mathrm{L=1}} = f_{\mathrm{GLo1}}^{E1} + f_{\mathrm{GLo2}}^{E1} + f_{\mathrm{SLo1}}^{E1} + f_{\mathrm{SLo2}}^{E1} + f_{\mathrm{upbend}}^{M1}, \quad (12)$$

with parameters $[E_{\mathrm{GLo1}}, E_{\mathrm{GLo2}}] = [18.1(1), 21.7(1)]$ MeV; $[\sigma_{\mathrm{GLo1}}, \sigma_{\mathrm{GLo2}}] = [72(1), 14(1)]$ mb; $[\Gamma_{\mathrm{GLo1}}, \Gamma_{\mathrm{GLo2}}] = [4.2(1), 1.7(2)]$ MeV; $T_f = 0.0(16)$ MeV; $[E_{\mathrm{SLo1}}, E_{\mathrm{SLo2}}] = [6.4(2), 13.8(4)]$ MeV; $[\sigma_{\mathrm{SLo1}}, \sigma_{\mathrm{SLo2}}] = [1.5(5), 9(1)]$ mb; $[\Gamma_{\mathrm{SLo1}}, \Gamma_{\mathrm{SLo2}}] = [1.3(3), 5(1)]$ MeV; $C = 2.2^{+1.8}_{-0.6} \cdot 10^{-8}$ MeV^{-3}; $\eta = 1.0(2)$ MeV^{-1}. Altogether, 15 free parameters were used in the fit, and they were fitted to all available data within the range $E_\gamma = 1.4$–25.0 MeV. We applied restrictions on the T_f and the Γ_{SLo2} parameter, where $T_f \in [0.0, 1.3]$ MeV and $\Gamma_{\mathrm{SLo2}} \in [0.0, 5.0]$ MeV.

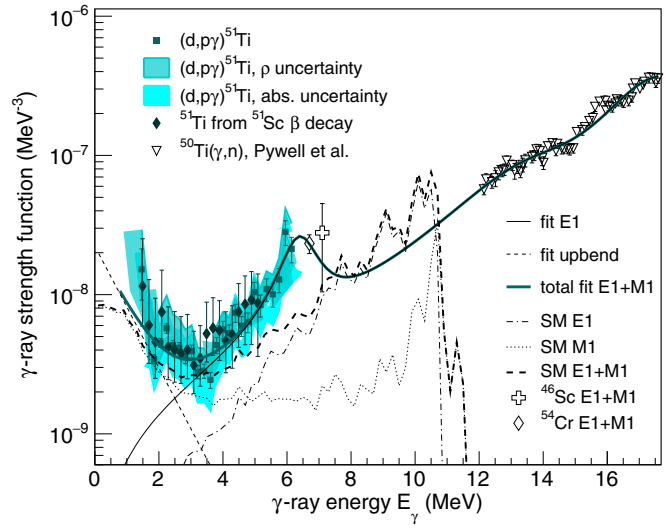

FIG. 5. Normalized γ-ray strength function of ^{51}Ti from the (d, p) and β-decay data. For the (d, p) data, the uncertainties are broken down to the statistical plus systematic errors from unfolding and extraction of primary γ rays (error bars on data points), uncertainties due to normalization of ρ (dark, cyan band), and absolute-scaling uncertainties (light, cyan band). The bin widths are 200 keV/channel for the β-decay data and 195 keV/channel for the (d, p) data. Also shown are the data from Pywell *et al.* [69] and strength functions of ^{46}Sc and ^{54}Cr as evaluated by Kopecky in RIPL-2 [28]. The fitted $E1$ and $M1$ components for the middle normalization of both the NLD and γSF are shown as a solid black line ($E1$), dashed black line ($M1$ upbend), and a solid, thick blue line ($E1 + M1$). The dashed-dotted line, the dotted line, and the thick dashed-dotted line show the $E1$, $M1$ and $E1 + M1$ contribution to the γSF obtained from shell-model calculations in comparison with the data. The neutron separation energy in ^{51}Ti is 6.372 MeV [79].

The resulting, normalized γ-ray strength function is shown in Fig. 5. For the (d, p) data, the various contributions to the total uncertainties are shown separately: error bars on the data points display statistical errors plus errors from unfolding and extraction of primary γ rays, while uncertainties due to the NLD normalization and the absolute scaling of the γ-ray strength are shown as shaded bands. The error bars shown for the β-decay data include statistical errors, systematic errors from the unfolding and extraction of primary γ rays, and systematic errors from the absolute normalization. The photodissociation data from from Pywell *et al.* [69] and the strength functions from the Reference Input Parameter Library (RIPL) version 2 [28] for ^{46}Sc and ^{54}Cr are also shown (Table I). Using our normalization approach, we obtain an average, total radiative width $\langle\Gamma_{\gamma 0}\rangle \approx 1240$ meV for the middle normalization (fully consistent with the RIPL-2 value of 1100(300) meV [28]), a maximum of $\langle\Gamma_{\gamma 0}^{\mathrm{max}}\rangle \approx 1960$ meV,

and a minimum of $\langle\Gamma_{\gamma 0}^{\min}\rangle \approx 740$ meV. These values are fully compatible with $\langle\Gamma_{\gamma 0}\rangle$ values in this mass region [29]; for example, $(n,\gamma)^{49}$Ti gives $\langle\Gamma_{\gamma 0}\rangle = 2300(140)$ meV, $(n,\gamma)^{47}$Ti gives $\langle\Gamma_{\gamma 0}\rangle = 1400(400)$ meV, and $(n,\gamma)^{50}$Ti has $\langle\Gamma_{\gamma 0}\rangle = 810(240)$ meV.

We note that in nuclei further from stability, the absence of any experimental $E1$ data near the separation energy for the nucleus under study requires a different approach for absolute normalization, such as reliance on theoretical models or information from neighboring nuclei as was done recently done in the Ni region [16,34].

IV. RESULTS AND DISCUSSION

To further investigate the suitability of the level-density and γSF normalization, configuration-interaction shell model calculations were performed using the KSHELL code [80]. We applied the SDPF-MU interaction [81], which comprises the full $2s1d$ and $2p1f$ shells, and the interaction matrix elements for the latter are based on GXPF1. With this model space, both parities are available, and we calculated 100 levels for each spin up to and including $15/2$ for both parities. For this model space, it was necessary to apply a $1\hbar\omega$ truncation, meaning that we only allowed basis elements with at most one particle-hole excitation over the sd-pf shell gap. With this truncation, the m-scheme dimension was 2.6×10^6 for positive parity and 2.0×10^8 for negative parity. The shell-model level density is shown as crosses in Fig. 4 and it is seen to agree very well with known, discrete levels as well as the present data sets.

For the γSF extraction, the $M1$ component was calculated using the GXPF1a interaction [82], which comprises the full $2p1f$ shell. No truncation was applied for the calculation, bringing the m-scheme dimension to 2.6×10^6. One hundred levels for each spin up to and including $29/2$ were calculated. All possible $M1$ transitions between levels were determined and included in the extraction of the γSF. The γSF was extracted from the calculations using the relation

$$f_{X1}(E_\gamma, E_i, J_i, \pi_i) = a_{X1}\langle B_{X1}\rangle(E_\gamma, E_i, J_i, \pi_i)\rho(E_i, J_i, \pi_i),$$

where $a_{M1} = 11.5473 \times 10^{-9}\,\mu_N^{-2}\,\mathrm{MeV}^{-2}$, $a_{E1} = 1.047 \times 10^{-6}\,e^{-2}\,\mathrm{fm}^{-2}\,\mathrm{MeV}^{-2}$, and $\rho(E_i, J_i, \pi_i)$ and $\langle B(X1)\rangle$ are the partial level density and the average reduced transition strength, respectively, of states with the given excitation energy, spin and parity. Using the generalized Brink-Axel hypothesis, $f_{XL}(E_\gamma, E_i, J_i, \pi_i) \approx f_{XL}(E_\gamma)$. Hence $f_{X1}(E_\gamma)$ was obtained by averaging over E_i, J_i, and π_i where only E_i, J_i, π_i states where f_{M1} is allowed are included in the average.

The $E1$ component was calculated with the SDPF-MU interaction [81] which required the inclusion of the next major shell to achieve the parity change between initial and final states. All $E1$ transitions between all levels were determined and included in the γSF extraction. The Lawson method [83] with a β parameter of 20 MeV was used to avoid spurious center-of-mass states [84–87]. The result is shown as the dashed-dotted ($E1$) and dotted ($M1$) lines in Fig. 5.

The shell-model calculations clearly support an assertion of $M1$ character for the low-energy upbend, in accordance with other recent shell-model work [88–92]. In the case of ^{56,57}Fe, there is experimental evidence that the upbend is dominated by dipole transitions [46,93]. Also, a recent paper by Jones *et al.* presenting Compton polarization measurements of transitions in the upbend region of ^{56}Fe, demonstrate a small bias towards $M1$ transitions being dominant [47]. Assuming magnetic character of the low-energy increase is also consistent with a new study by Krtička *et al.* [94] of neutron-resonance data for a wide range of nuclei measured with the DANCE detector.

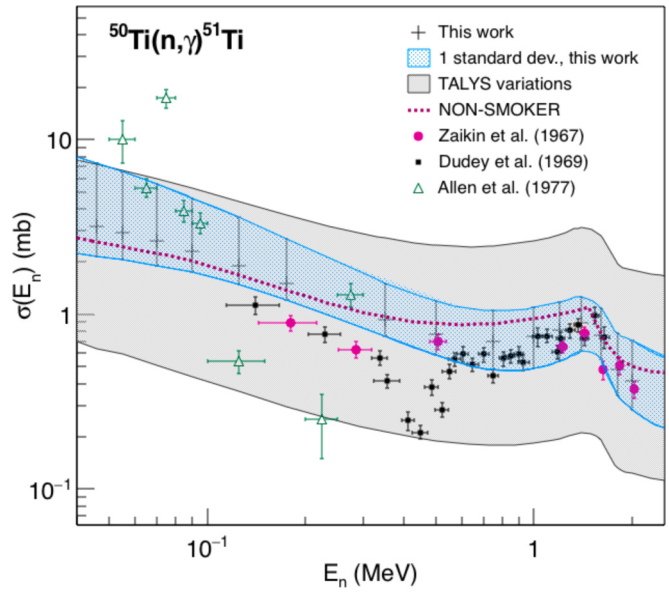

FIG. 6. Experimental ^{50}Ti (n,γ) ^{51}Ti cross section taken from Refs. [97–100], shown by the points, compared to the cross section constrained using the β decay of ^{51}Sc and from the ^{50}Ti$(d,p)^{51}$Ti reaction data as input into a TALYS calculation. The blue-shaded error band shows the one-standard deviation on the cross section, including uncertainties from the width-fluctuation model, the two different n-OMPs and the direct capture contribution (only in the upper one-σ limit). The gray band shows the maximum and minimum TALYS predictions varying the input models for the level density, γSF, and neutron optical model. The different NLD models were not normalized to D_0 in the TALYS calculations.

We observe that the shell-model calculations reproduce excellently the overall shape of the γ-ray strength function data. The absolute value of the shell-model calculations is at the lower end of the estimated error bars. It should be emphasized that the two widely different experimental techniques and population mechanisms, β decay and (d,p) reactions, provide equivalent NLDs and γSFs when analyzed and normalized in a consistent manner.

The extracted NLD and γSF from both the (d,p) data and the β-decay data are applied as input to the Hauser-Feshbach code TALYS-1.9 [95,96] to constrain the ^{50}Ti$(n,\gamma)^{51}$Ti rate provided in Fig. 6. More specifically, for the NLD, we used the first 14 known, discrete levels of ^{51}Ti up to $E_x = 3.2$ MeV, and above that energy we used the constant-temperature model with parameters as described in Sec. III corresponding to the low, middle, and high normalizations [$\rho(S_n) = 91, 146, 248\ \mathrm{MeV}^{-1}$]. Furthermore, for the γSF, we created tabulated values of the fit function given in Eq. (12) for all

the various normalization options and used those as input to TALYS.

Although the NLD and γSF impact most the calculated (n, γ) cross section, other parameters contribute to the uncertainty as well. Therefore, both the optical model of Jeukenne-Lejeune-Mahaux (JLM) type [101] and the phenomenological potential from Ref. [102] were tested and their (small) variation in the predicted cross section are included in the estimated uncertainty band. Moreover, two approaches for calculating width fluctuations are considered: the usual Moldauer expression [103,104] and the Hofmann-Richert-Tepel-Weidenmüller model [105–107]. In addition, a possible direct-capture contribution is estimated by using the prescription of Ref. [108]. To estimate one-standard-deviation errors, we calculated the (n, γ) cross section varying each uncertainty parameter one at a time and derived the deviation relative to the recommended (middle) normalization. For each incoming neutron energy E_n in the calculation energy grid, the upper uncertainty $\delta_{\mathrm{err,high}}$ of the data-constrained cross section σ_{rec} is calculated as

$$\delta^2_{\mathrm{err,high}} = \sigma^2_{\mathrm{rec}}\left[\left(\frac{\sigma_{\mathrm{wf}}-\sigma_{\mathrm{rec}}}{\sigma_{\mathrm{rec}}}\right)^2+\left(\frac{\sigma_{\mathrm{nOMP}}-\sigma_{\mathrm{rec}}}{\sigma_{\mathrm{rec}}}\right)^2+\left(\frac{\sigma_{\mathrm{NLDup}}-\sigma_{\mathrm{rec}}}{\sigma_{\mathrm{rec}}}\right)^2+\left(\frac{\sigma_{\gamma\mathrm{SFup}}-\sigma_{\mathrm{rec}}}{\sigma_{\mathrm{rec}}}\right)^2+\left(\frac{\sigma_{\mathrm{DC}}-\sigma_{\mathrm{rec}}}{\sigma_{\mathrm{rec}}}\right)^2\right].$$

Here, σ_{rec} represents the recommended cross section using the middle normalization of the NLD and γSF, the default optical potential of Ref. [102], and the default Moldauer expression for the width-fluctuation correction. Furthermore, σ_{wf} is obtained by using the Hofmann-Richert-Tepel-Weidenmüller model for the width fluctuation correction, and σ_{nOMP} using the JLM neutron optical-model potential. Finally, σ_{NLDup} is calculated using the upper NLD normalization, $\sigma_{\gamma\mathrm{SFup}}$ with the upper γSF normalization, and σ_{DC} is calculated by including the direct-capture contribution. Similarly, the lower uncertainty $\delta_{\mathrm{err,low}}$ is estimated by

$$\delta^2_{\mathrm{err,low}} = \sigma^2_{\mathrm{rec}}\left[\left(\frac{\sigma_{\mathrm{wf}}-\sigma_{\mathrm{rec}}}{\sigma_{\mathrm{rec}}}\right)^2+\left(\frac{\sigma_{\mathrm{nOMP}}-\sigma_{\mathrm{rec}}}{\sigma_{\mathrm{rec}}}\right)^2+\left(\frac{\sigma_{\mathrm{NLDlow}}-\sigma_{\mathrm{rec}}}{\sigma_{\mathrm{rec}}}\right)^2+\left(\frac{\sigma_{\gamma\mathrm{SFlow}}-\sigma_{\mathrm{rec}}}{\sigma_{\mathrm{rec}}}\right)^2\right].$$

Note that we have not included the direct-capture contribution here, as this term will only provide an increase in the cross section and not a reduction. Further, as the NLD and γSF normalizations are also not symmetric, it was necessary to estimate the lower and upper uncertainties separately.

The experimentally constrained cross section is compared to existing experimental data [98–100] and a NON-SMOKER calculation [109,110]. For such a light-mass nucleus with a relatively low level density, the comparison between the previously measured values and the present cross section is reasonable. There appears to be some resonancelike behavior in the experimentally measured capture cross section at lower energies which is not captured in the present measurement since the treatment of the NLD and γSF within TALYS will lead to an *average* cross section. Above $E_n \approx 0.6$ MeV, the agreement is excellent.

The uncertainty in the cross section extracted for the ^{50}Ti neutron capture cross section is roughly a factor of 2. For the neutron-energy range $E_n \simeq 0.6$–2 MeV, where the Hauser-Feshbach model is considered applicable for this light target nucleus, our experimentally guided calculations present a significant improvement compared to the TALYS predictions for which all input models are varied. As an example of the applicability of such neutron capture rates, astrophysical sensitivity studies [17,111] have called for determining neutron capture rates of short-lived isotopes with errors less than an order of magnitude and this appears achievable with the β-Oslo technique. Current r-process simulations for a neutron-star merger scenario indicate temperatures of the range ∼0.1–10 GK [9,10], corresponding to neutron energies of ∼0.01–1 MeV. For these energies, especially for neutron captures taking place at freeze-out, most nuclei in the r-process reaction network would have sufficiently high neutron separation energies, and thus high level densities, so that the Hauser-Feshbach treatment applies [112].

V. SUMMARY AND CONCLUSIONS

In summary, the NLD and γSF function of ^{51}Ti have been independently determined following the β decay of ^{51}Sc and the (d, p) reaction on ^{50}Ti and are in excellent agreement. The neutron capture cross section of ^{50}Ti was constrained based on the measured NLD and γSF and compared to previously measured direct neutron capture data. For incoming neutrons above ≈0.6 MeV, the close match between the β-Oslo and Oslo methods with the direct measurements validates the newly developed β-Oslo method for the determination of neutron capture cross sections. Hence, the β-Oslo method provides a new tool for the extraction of neutron capture cross sections far from stability that are difficult to obtain otherwise.

ACKNOWLEDGMENTS

This research was supported by Michigan State University and the Facility for Rare Isotope Beams and was funded in part by the NSF under Contracts No. PHY-1102511 (NSCL), No. 1350234 (CAREER), No. 1430152 (JINA-CEE), No. 0822648, and No. 1419765 (M.M. and R.S.), and the US Department of Energy under Contracts No. DE-SC0013039 (R.S.) and No. DE-AC52-07NA27344 (LLNL), and the National Nuclear Security Administration under Awards No. DE-NA0000979, No. DE-NA0003180, and No. DE-NA0003221 and Grant No. DE-FC03-03NA00143. G.P. would like to acknowledge support from the College of Science and Technology of Central Michigan University. A.C.L. gratefully acknowledges funding from the ERC-STG-2014 under Grant Agreement No. 637686, and support from the "ChETEC" COST Action (CA16117), supported by COST (European Cooperation in Science and Technology). G.M.T. gratefully acknowledges funding of this research from the Research Council of Norway, Project Grant No. 222287. M.W. acknowledges support from the National Research Foundation

of South Africa under Grant No. 92789. The authors wish to thank J. C. Müller, A. Semchenkov, and J. C. Wikne at the Oslo Cyclotron Laboratory for providing excellent experimental conditions.

[1] E. M. Burbidge, G. R. Burbidge, W. A. Fowler, and F. Hoyle, Rev. Mod. Phys. **29**, 547 (1957).
[2] M. Arnould, S. Goriely, and K. Takahashi, Phys. Rep. **450**, 97 (2007).
[3] B. P. Abbott *et al.*, Phys. Rev. Lett. **119**, 161101 (2017).
[4] D. A. Coulter *et al.*, Science **358**, 1556 (2017).
[5] S. Valenti, David, J. Sand, S. Yang, E. Cappellaro, L. Tartaglia, A. Corsi, S. W. Jha, D. E. Reichart, J. Haislip, and V. Kouprianov, Astrophys. J. **848**, L24 (2017).
[6] E. Pian *et al.*, Nature (London) **551**, 67 (2017).
[7] M. R. Drout *et al.*, Science **358**, 1570 (2017).
[8] D. Kasen, B. D. Metzger, J. Barnes, E. Quataert, and E. Ramirez-Ruiz, Nature (London) **551**, 80 (2017).
[9] S. Goriely, A. Bauswein, and H.-T. Janka, Astrophys. J. Lett. **738**, L32 (2011).
[10] J. de Jesús Mendoza-Temis, M. R. Wu, K. Langanke, G. Martinez-Pinedo, A. Bauswein, and H. T. Janka, Phys. Rev. C **92**, 055805 (2015).
[11] D. Clayton, Astrophys. J. **139**, 637 (1964).
[12] M. Mosconi, K. Fujii, A. Mengoni, C. Domingo-Pardo, F. Käppeler, U. Abbondanno, G. Aerts, H. Álvarez-Pol, F. Alvarez-Velarde, S. Andriamonje, J. Andrzejewski, P. Assimakopoulos, L. Audouin, G. Badurek, P. Baumann, F. Bečvář, F. Belloni, E. Berthoumieux, S. Bisterzo, M. Calviani *et al.* (The nTOF Collaboration), Phys. Rev. C **82**, 015802 (2010).
[13] G. Aliberti, G. Palmiotti, M. Salvatores, T. Kim, T. Taiwo, M. Anitescu, I. Kodeli, E. Sartori, J. Bosq, and J. Tommasi, Ann. Nucl. Energy **33**, 700 (2006).
[14] N. Colonna, F. Belloni, E. Berthoumieux, M. Calviani, C. Domingo-Pardo, C. Guerrero, D. Karadimos, C. Lederer, C. Massimi, C. Paradela, R. Plag, J. Praena, and R. Sarmento, Energy Environ. Sci. **3**, 1910 (2010).
[15] Accelerator Driven Systems and Fast Reactors in Advanced Nuclear Fuel Cycles, ISBN 92-64-18482-1 ENEA/OECD Report, 2002 .
[16] S. N. Liddick, A. Spyrou, B. P. Crider, F. Naqvi, A. C. Larsen, M. Guttormsen, M. Mumpower, R. Surman, G. Perdikakis, D. L. Bleuel, A. Couture, L. Crespo Campo, A. C. Dombos, R. Lewis, S. Mosby, S. Nikas, C. J. Prokop, T. Renstrøm, B. Rubio, S. Siem, and S. J. Quinn, Phys. Rev. Lett. **116**, 242502 (2016).
[17] R. Surman and J. Engel, Phys. Rev. C **64**, 035801 (2001).
[18] H. Utsunomiya, S. Goriely, H. Akimune, H. Harada, F. Kitatani, S. Goko, H. Toyokawa, K. Yamada, T. Kondo, O. Itoh, M. Kamata, T. Yamagata, Y.-W. Lui, I. Daoutidis, D. P. Arteaga, S. Hilaire, and A. J. Koning, Phys. Rev. C **82**, 064610 (2010).
[19] J. E. Escher, J. T. Burke, F. S. Dietrich, N. D. Scielzo, I. J. Thompson, and W. Younes, Rev. Mod. Phys. **84**, 353 (2012).
[20] J. E. Escher, J. T. Burke, R. O. Hughes, N. D. Scielzo, R. J. Casperson, S. Ota, H. I. Park, A. Saastamoinen, and T. J. Ross, Phys. Rev. Lett. **121**, 052501 (2018).
[21] M. Guttormsen, T. Ramsøy, and J. Rekstad, Nucl. Instrum. Methods Phys. Res., Sect. A **255**, 518 (1987).
[22] A. Schiller, L. Bergholt, M. Guttormsen, E. Melby, J. Rekstad, and S. Siem, Nucl. Instrum. Methods Phys. Res., Sect. A **447**, 498 (2000).
[23] A. Spyrou, S. N. Liddick, A. C. Larsen, M. Guttormsen, K. Cooper, A. C. Dombos, D. J. Morrissey, F. Naqvi, G. Perdikakis, S. J. Quinn, T. Renstrøm, J. A. Rodriguez, A. Simon, C. S. Sumithrarachchi, and R. G. T. Zegers, Phys. Rev. Lett. **113**, 232502 (2014).
[24] K. L. Jones, A. S. Adekola, D. Bardayan, J. Blackmon, K. Chae, K. Chipps, J. Cizewski, L. Erikson, C. Harlin, R. Hatarik, R. Kapler, R. Kozub, J. Liang, Z. M. R. Livesay, B. Moazen, C. Nesaraja, F. Nunes, S. Pain, N. Patterson, D. Shapira, J. Shriner, M. Smith, T. Swan, and J. Thomas, Nature (London) **465**, 454 (2010).
[25] A. C. Larsen, M. Guttormsen, R. Schwengner, D. L. Bleuel, S. Goriely, S. Harissopulos, F. L. Bello Garrote, Y. Byun, T. K. Eriksen, F. Giacoppo, A. Görgen, T. W. Hagen, M. Klintefjord, T. Renstrøm, S. J. Rose, E. Sahin, S. Siem, T. G. Tornyi, G. M. Tveten, A. V. Voinov, and M. Wiedeking, Phys. Rev. C **93**, 045810 (2016).
[26] A. C. Larsen and S. Goriely, Phys. Rev. C **82**, 014318 (2010).
[27] S. I. Al-Quraishi, S. M. Grimes, T. N. Massey, and D. A. Resler, Phys. Rev. C **63**, 065803 (2001).
[28] T. Belgya, O. Bersillon, R. Capote, T. Fukahori, G. Zhigang, S. Goriely, M. Herman, A.V. Ignatyuk, S. Kailas, A. Koning, P. Oblozinsky, V. Plujko and P. Young., *Handbook for calculations of nuclear reaction data*, RIPL-2. IAEA-TECDOC-1506 (IAEA, Vienna, 2006) available online at https://www-nds.iaea.org/ripl-2/.
[29] R. Capote, M. Herman, P. Obložinský, P. Young, S. Goriely, T. Belgya, A. Ignatyuk, A. Koning, S. Hilaire, V. Plujko, M. Avrigeanu, O. Bersillon, M. Chadwick, T. Fukahori, Z. Ge, Y. Han, S. Kailas, J. Kopecky, V. Maslov, G. Reffo, M. Sin, E. Soukhovitskii, and P. Talou, Nucl. Data Sheets **110**, 3107 (2009), Special Issue on Nuclear Reaction Data.
[30] H. Utsunomiya, S. Goriely, T. Kondo, C. Iwamoto, H. Akimune, T. Yamagata, H. Toyokawa, H. Harada, F. Kitatani, Y.-W. Lui, A. C. Larsen, M. Guttormsen, P. E. Koehler, S. Hilaire, S. Péru, M. Martini, and A. J. Koning, Phys. Rev. C **88**, 015805 (2013).
[31] T. G. Tornyi, M. Guttormsen, T. K. Eriksen, A. Görgen, F. Giacoppo, T. W. Hagen, A. Krasznahorkay, A. C. Larsen, T. Renstrøm, S. J. Rose, S. Siem, and G. M. Tveten, Phys. Rev. C **89**, 044323 (2014).
[32] T. A. Laplace, F. Zeiser, M. Guttormsen, A. C. Larsen, D. L. Bleuel, L. A. Bernstein, B. L. Goldblum, S. Siem, F. L. Bello Garotte, J. A. Brown, L. C. Campo, T. K. Eriksen, F. Giacoppo, A. Görgen, K. Hadyńska-Klwk, R. A. Henderson, M. Klintefjord, M. Lebois, T. Renstrøm, S. J. Rose, E. Sahin, T. G. Tornyi, G. M. Tveten, A. Voinov, M. Wiedeking, J. N. Wilson, and W. Younes, Phys. Rev. C **93**, 014323 (2016).
[33] B. V. Kheswa, M. Wiedeking, J. A. Brown, A. C. Larsen, S. Goriely, M. Guttormsen, F. L. Bello Garrote, L. A. Bernstein, D. L. Bleuel, T. K. Eriksen, F. Giacoppo, A. Görgen, B. L. Goldblum, T. W. Hagen, P. E. Koehler, M. Klintefjord, K. L. Malatji, J. E. Midtbø, H. T. Nyhus, P. Papka, T. Renstrøm, S. J.

Rose, E. Sahin, S. Siem, and T. G. Tornyi, Phys. Rev. C **95**, 045805 (2017).
[34] A. Spyrou, A. C. Larsen, S. N. Liddick, F. Naqvi, B. P. Crider, A. C. Dombos, M. Guttormsen, D. L. Bleuel, A. Couture, L. C. Campo, R. Lewis, S. Mosby, M. R. Mumpower, G. Perdikakis, C. J. Prokop, S. J. Quinn, T. Renstrøm, S. Siem, and R. Surman, J. Phys. G: Nucl. Part. Phys. **44**, 044002 (2017).
[35] D. J. Morrissey, B. M. Sherrill, M. Steiner, A. Stolz, and I. Wiedenhoever, Nucl. Instrum. Methods Phys. Res. B **204**, 90 (2003).
[36] A. Simon, S. Quinn, A. Spyrou, A. Battaglia, I. Beskin, A. Best, B. Bucher, M. Couder, P. DeYoung, X. Fang, J. Görres, A. Kontos, Q. Li, S. Liddick, A. Long, S. Lyons, K. Padmanabhan, J. Peace, A. Roberts, D. Robertson, K. Smith, M. Smith, E. Stech, B. Stefanek, W. Tan, X. Tang, and M. Wiescher, Nucl. Instrum. Methods Phys. Res., Sect. A **703**, 16 (2013).
[37] C. N. Davids, S. L. Tabor, E. B. Norman, R. C. Pardo, and L. A. Parks, Phys. Rev. C **14**, 1601 (1976).
[38] T. Ishimori, K. Ueno, M. Hoshi, M. Saeki, and K. Awa, JAERI Technical Report No. 1178 P 5, 1969.
[39] M. E. Bunker and J. W. Starner, Phys. Rev. **97**, 1272 (1955).
[40] B. W. Sargent, L. Yaffe, and A. P. Gray, Can. J. Phys. **31**, 235 (1953).
[41] N. N. D. C. Q. value calculator, (2016).
[42] M. Guttormsen, A. Bürger, T. Hansen, and N. Lietaer, Nucl. Instrum. Methods Phys. Res., Sect. A **648**, 168 (2011).
[43] M. Guttormsen, A. Atac, G. Løvhøiden, S. Messelt, T. Ramsøy, J. Rekstad, T. F. Thorsteinsen, T. S. Tveter, and Z. Zelazny, Phys. Scr. **T32**, 54 (1990).
[44] M. Guttormsen, T. Tveter, L. Bergholt, F. Ingebretsen, and J. Rekstad, Nucl. Instrum. Methods Phys. Res., Sect. A **374**, 371 (1996).
[45] A. C. Larsen, M. Guttormsen, M. Krtička, E. Běták, A. Bürger, A. Görgen, H. T. Nyhus, J. Rekstad, A. Schiller, S. Siem, H. K. Toft, G. M. Tveten, A. V. Voinov, and K. Wikan, Phys. Rev. C **83**, 034315 (2011).
[46] A. C. Larsen, N. Blasi, A. Bracco, F. Camera, T. K. Eriksen, A. Görgen, M. Guttormsen, T. W. Hagen, S. Leoni, B. Million, H. T. Nyhus, T. Renstrøm, S. J. Rose, I. E. Ruud, S. Siem, T. Tornyi, G. M. Tveten, A. V. Voinov, and M. Wiedeking, Phys. Rev. Lett. **111**, 242504 (2013).
[47] M. D. Jones, A. O. Macchiavelli, M. Wiedeking, L. A. Bernstein, H. L. Crawford, C. M. Campbell, R. M. Clark, M. Cromaz, P. Fallon, I. Y. Lee, M. Salathe, A. Wiens, A. D. Ayangeakaa, D. L. Bleuel, S. Bottoni, M. P. Carpenter, H. M. Davids, J. Elson, A. Görgen, M. Guttormsen, R. V. F. Janssens, J. E. Kinnison, L. Kirsch, A. C. Larsen, T. Lauritsen, W. Reviol, D. G. Sarantites, S. Siem, A. V. Voinov, and S. Zhu, Phys. Rev. C **97**, 024327 (2018).
[48] D. Brink, doctoral thesis, Oxford University, 1955.
[49] P. Axel, Phys. Rev. **126**, 671 (1962).
[50] M. Guttormsen, A. C. Larsen, A. Görgen, T. Renstrøm, S. Siem, T. G. Tornyi, and G. M. Tveten, Phys. Rev. Lett. **116**, 012502 (2016).
[51] L. C. Campo, M. Guttormsen, F. L. B. Garrote, T. K. Eriksen, F. Giacoppo, A. Görgen, K. Hadynska-Klek, M. Klintefjord, A. C. Larsen, T. Renstrøm, E. Sahin, S. Siem, A. Springer, T. G. Tornyi, and G. M. Tveten, Phys. Rev. C **98**, 054303 (2018).
[52] C. E. Porter and R. G. Thomas, Phys. Rev. **104**, 483 (1956).
[53] National Nuclear Data Center at www.nndc.bnl.gov (2019).
[54] T. Ericson, Nucl. Phys. **11**, 481 (1959).
[55] A. Gilbert and A. G. W. Cameron, Can. J. Phys. **43**, 1446 (1965).
[56] A. V. Voinov, B. M. Oginni, S. M. Grimes, C. R. Brune, M. Guttormsen, A. C. Larsen, T. N. Massey, A. Schiller, and S. Siem, Phys. Rev. C **79**, 031301(R) (2009).
[57] K.-H. Schmidt and B. Jurado, Phys. Rev. Lett. **104**, 212501 (2010).
[58] M. Guttormsen, B. Jurado, J. N. Wilson, M. Aiche, L. A. Bernstein, Q. Ducasse, F. Giacoppo, A. Görgen, F. Gunsing, T. W. Hagen, A. C. Larsen, M. Lebois, B. Leniau, T. Renstrøm, S. J. Rose, S. Siem, T. Tornyi, G. M. Tveten, and M. Wiedeking, Phys. Rev. C **88**, 024307 (2013).
[59] M. Guttormsen, A. C. Larsen, F. L. Bello Garrote, Y. Byun, T. K. Eriksen, F. Giacoppo, A. Görgen, T. W. Hagen, M. Klintefjord, H. T. Nyhus, T. Renstrøm, S. J. Rose, E. Sahin, S. Siem, T. Tornyi, G. M. Tveten, and A. Voinov, Phys. Rev. C **90**, 044309 (2014).
[60] M. Guttormsen, M. Aiche, F. L. B. Garrote, L. A. Bernstein, D. L. Bleuel, Y. Byun, Q. Ducasse, T. K. Eriksen, F. Giacoppo, A. Görgen, F. Gunsing, T. W. Hagen, B. Jurado, M. Klintefjord, A. C. Larsen, L. Lebois, B. Leniau, H. T. Nyhus, T. Renstrøm, S. J. Rose, E. Sahin, S. Siem, T. G. Tornyi, G. M. Tveten, A. Voinov, M. Wiedeking, and J. Wilson, Eur. Phys. J. A **51**, 170 (2015).
[61] N. Dinh Dang, N. Quang Hung, and L. T. Quynh Huong, Phys. Rev. C **96**, 054321 (2017).
[62] T. Renstrøm, H. Utsunomiya, H. T. Nyhus, A. C. Larsen, M. Guttormsen, G. M. Tveten, D. M. Filipescu, I. Gheorghe, S. Goriely, S. Hilaire, Y.-W. Lui, J. E. Midtbø, S. Péru, T. Shima, S. Siem, and O. Tesileanu, Phys. Rev. C **98**, 054310 (2018).
[63] R. Ginaven, A. Bernstein, R. Drisko, and J. McGrory, Phys. Lett. B **25**, 206 (1967).
[64] T. von Egidy and D. Bucurescu, Phys. Rev. C **80**, 054310 (2009).
[65] M. Guttormsen *et al.*, Phys. Rev. C **96**, 024313 (2017).
[66] T. von Egidy and D. Bucurescu, Phys. Rev. C **72**, 044311 (2005).
[67] M. Chadwick *et al.*, IAEA-TECDOC, 1998.
[68] S. F. Mughabghab, *Atlas of Neutron Resonances*, 6th ed. (Elsevier, Amsterdam, 2018).
[69] R. Pywell, M. Thompson, and R. Hicks, Nucl. Phys. A **325**, 116 (1979).
[70] J. M. Blatt and V. F. Weisskopf, in *Theoretical Nuclear Physics* (John Wiley & Sons, New York, 1952), p. 530.
[71] J. Kopecky and R. E. Chrien, Nucl. Phys. A **468**, 285 (1987).
[72] J. Kopecky and M. Uhl, Phys. Rev. C **41**, 1941 (1990).
[73] C. Djalali, N. Marty, M. Morlet, A. Willis, J. Jourdain, N. Anantaraman, G. M. Crawley, A. Galonsky, and J. Duffy, Nucl. Phys. A **410**, 399 (1983).
[74] C. Djalali, N. Marty, M. Morlet, A. Willis, J. Jourdain, N. Anantaraman, G. M. Crawley, A. Galonsky, and P. Kitching, Nucl. Phys. A **388**, 1 (1982).
[75] A. Voinov, E. Algin, U. Agvaanluvsan, T. Belgya, R. Chankova, M. Guttormsen, G. E. Mitchell, J. Rekstad, A. Schiller, and S. Siem, Phys. Rev. Lett. **93**, 142504 (2004).

[76] A. C. Larsen, S. Goriely, A. Bürger, M. Guttormsen, A. Görgen, S. Harissopulos, M. Kmiecik, T. Konstantinopoulos, A. Lagoyannis, T. Lönnroth, K. Mazurek, M. Norrby, H. T. Nyhus, G. Perdikakis, A. Schiller, S. Siem, A. Spyrou, N. U. H. Syed, H. K. Toft, G. M. Tveten, and A. Voinov, Phys. Rev. C **85**, 014320 (2012).
[77] N. U. H. Syed, A. C. Larsen, A. Bürger, M. Guttormsen, S. Harissopulos, M. Kmiecik, T. Konstantinopoulos, M. Krtička, A. Lagoyannis, T. Lönnroth, K. Mazurek, M. Norby, H. T. Nyhus, G. Perdikakis, S. Siem, and A. Spyrou, Phys. Rev. C **80**, 044309 (2009).
[78] K. Sieja (unpublished).
[79] M. Wang, G. Audi, F. Kondev, W. Huang, S. Naimi, and X. Xu, Chin. Phys. C **41**, 030003 (2017).
[80] N. Shimizu, *Nuclear shell-model code for massive parallel computation*, "KSHELL" Noritaka Shimizu and arXiv:1310.5431.
[81] Y. Utsuno, T. Otsuka, B. A. Brown, M. Honma, T. Mizusaki, and N. Shimizu, Phys. Rev. C **86**, 051301(R) (2012).
[82] M. Honma, T. Otsuka, B. A. Brown, and T. Mizusaki, Phys. Rev. C **65**, 061301(R) (2002).
[83] C. W. Johnson, W. E. Ormand, K. S. McElvain, and H. Shan, arXiv:1801.08432.
[84] D. Gloeckner and R. Lawson, Phys. Lett. B **53**, 313 (1974).
[85] R. Lawson, *Theory of the Nuclear Shell Model* (Clarendon, Oxford, 1980).
[86] F. Palumbo, Nucl. Phys. A **99**, 100 (1967).
[87] F. Palumbo and D. Prosperi, Nucl. Phys. A **115**, 296 (1968).
[88] R. Schwengner, S. Frauendorf, and A. C. Larsen, Phys. Rev. Lett. **111**, 232504 (2013).
[89] B. A. Brown and A. C. Larsen, Phys. Rev. Lett. **113**, 252502 (2014).
[90] K. Sieja, Phys. Rev. Lett. **119**, 052502 (2017).
[91] R. Schwengner, S. Frauendorf, and B. A. Brown, Phys. Rev. Lett. **118**, 092502 (2017).
[92] A. C. Larsen, J. E. Midtbø, M. Guttormsen, T. Renstrøm, S. N. Liddick, A. Spyrou, S. Karampagia, B. A. Brown, O. Achakovskiy, S. Kamerdzhiev, D. L. Bleuel, A. Couture, L. C. Campo, B. P. Crider, A. C. Dombos, R. Lewis, S. Mosby, F. Naqvi, G. Perdikakis, C. J. Prokop, S. J. Quinn, and S. Siem, Phys. Rev. C **97**, 054329 (2018).
[93] A. C. Larsen, M. Guttormsen, N. Blasi, A. Bracco, F. Camera, L. C. Campo, T. K. Eriksen, A. Görgen, T. W. Hagen, V. W. Ingeberg, B. V. Kheswa, S. Leoni, J. E. Midtbø, B. Million, H. T. Nyhus, T. Renstrøm, S. J. Rose, I. E. Ruud, S. Siem, T. G. Tornyi, G. M. Tveten, A. V. Voinov, M. Wiedeking, and F. Zeiser, J. Phys. G: Nucl. Part. Phys. **44**, 064005 (2017).
[94] M. Krtička, S. Goriely, S. Hilaire, S. Péru, and S. Valenta, Phys. Rev. C **99**, 044308 (2019).
[95] O. Bersillon, F. Gunsing, E. Bauge, R. Jacqmin, and S. Leray, eds., *TALYS-1.6: Proceedings of the International Conference on Nuclear Data for Science and Technology 2007* (EDP Sciences, Nice, France, 2007).
[96] A. J. Koning and D. Rochman, Nucl. Data Sheets **113**, 2841 (2012).
[97] J. F. Vervier, Nucl. Phys. **9**, 569 (1959).
[98] G. Zaikin, I. Korzh, N. Skljar, and I. A. Totskij, Atomnaya Energiya **23**, 67 (1967).
[99] N. Dudey, R. Heinrich, and A. Madson, J. Nucl. Energy **23**, 443 (1969).
[100] B. Allen, J. Boldeman, A. D. Musgrove, and R. Macklin, Australian AEC Technical Report No. 402, 1977.
[101] E. Bauge, J. P. Delaroche, and M. Girod, Phys. Rev. C **63**, 024607 (2001).
[102] A. Koning and J. Delaroche, Nucl. Phys. A **713**, 231 (2003).
[103] P. A. Moldauer, Phys. Rev. C **14**, 764 (1976).
[104] P. A. Moldauer, Nucl. Phys. A **344**, 185 (1980).
[105] H. M. Hofmann, J. Richert, J. W. Tepel, and H. A. Weidenmüller, Ann. Phys. (NY) **90**, 403 (1975).
[106] J. W. Tepel, H. M. Hofmann, and H. A. Weidenmüller, Phys. Lett. B **49**, 1 (1974).
[107] H. M. Hofmann, T. Mertelmeier, M. Herman, and J. W. Tepel, Zeit. Phys. A **297**, 153 (1980).
[108] Y. Xu and S. Goriely, Phys. Rev. C **86**, 045801 (2012).
[109] T. Rauscher and F.-K. Thielemann, At. Data Nucl. Data Tables **75**, 1 (2000).
[110] R. H. Cyburt, A. M. Amthor, R. Ferguson, Z. Meisel, K. Smith, S. Warren, A. Heger, R. D. Hoffman, T. Rauscher, A. Sakharuk, H. Schatz, F. K. Thielemann, and M. Wiescher, Astrophys. J. Suppl. Ser. **189**, 240 (2010).
[111] M. Mumpower, R. Surman, G. McLaughlin, and A. Aprahamian, Prog. Part. Nucl. Phys. **86**, 86 (2016).
[112] T. Rauscher, F.-K. Thielemann, and K.-L. Kratz, Phys. Rev. C **56**, 1613 (1997).